Structure and Calcium-Binding Properties of Frq1, a Novel Calcium Sensor in the Yeast *Saccharomyces cerevisiae*†

James B. Ames,*,‡ Kristin B. Hendricks,§,# Thomas Strahl,§ Inken G. Huttner,§ Nobuko Hamasaki,‡ and Jeremy Thorner§

Center for Advanced Research in Biotechnology, University of Maryland Biotechnology Institute, Rockville, Maryland 20850, and Department of Molecular and Cell Biology, Division of Biochemistry and Molecular Biology, University of California, Berkeley, California 94720-3202

Received June 6, 2000; Revised Manuscript Received August 3, 2000

ABSTRACT: The *FRQ1* gene is essential for growth of budding yeast and encodes a 190-residue, N-myristoylated (myr) calcium-binding protein. Frq1 belongs to the recoverin/frequenin branch of the EF-hand superfamily and regulates a yeast phosphatidylinositol 4-kinase isoform. Conformational changes in Frq1 due to N-myristoylation and Ca^{2+} binding were assessed by nuclear magnetic resonance (NMR), fluorescence, and equilibrium Ca^{2+}-binding measurements. For this purpose, Frq1 and myr-Frq1 were expressed in and purified from *Escherichia coli*. At saturation, Frq1 bound three Ca^{2+} ions at independent sites, which correspond to the second, third, and fourth EF-hand motifs in the protein. Affinity of the second site ($K_d = 10\ \mu M$) was much weaker than that of the third and fourth sites ($K_d = 0.4\ \mu M$). Myr-Frq1 bound Ca^{2+} with a $K_d$app of 3 μM and a positive Hill coefficient ($n = 1.25$), suggesting that the N-myristoyl group confers some degree of cooperativity in Ca^{2+} binding, as seen previously in recoverin. Both the NMR and fluorescence spectra of Frq1 exhibited very large Ca^{2+}-dependent differences, indicating major conformational changes induced upon Ca^{2+} binding. Nearly complete sequence-specific NMR assignments were obtained for the entire carboxy-terminal domain (residues K100−I190). Assignments were made for 20% of the residues in the amino-terminal domain; unassigned residues exhibited very broad NMR signals, most likely due to Frq1 dimerization. NMR chemical shifts and nuclear Overhauser effect (NOE) patterns of Ca^{2+}-bound Frq1 were very similar to those of Ca^{2+}-bound recoverin, suggesting that the overall structure of Frq1 resembles that of recoverin. A model of the three-dimensional structure of Ca^{2+}-bound Frq1 is presented based on the NMR data and homology to recoverin. N-myristoylation of Frq1 had little or no effect on its NMR and fluorescence spectra, suggesting that the myristoyl moiety does not significantly alter Frq1 structure. Correspondingly, the NMR chemical shifts for the myristoyl group in both Ca^{2+}-free and Ca^{2+}-bound myr-Frq1 were nearly identical to those of free myristate in solution, indicating that the fatty acyl chain is solvent-exposed and not sequestered within the hydrophobic core of the protein, unlike the myristoyl group in Ca^{2+}-free recoverin. Subcellular fractionation experiments showed that both the N-myristoyl group and Ca^{2+}-binding contribute to the ability of Frq1 to associate with membranes.

Calcium ion (Ca^{2+}) regulates many important physiological processes in the budding yeast, *Saccharomyces cerevisiae* (reviewed in ref *1*), as it does in other eukaryotic cell types (reviewed in ref *2*). Moreover, the yeast genome encodes channels (*3*) and pumps (*4*) homologous to those involved in regulated Ca^{2+} entry and maintenance of Ca^{2+} homeostasis in mammalian cells. In all eukaryotic cells, the effects of changes in intracellular Ca^{2+} levels are mediated primarily by small Ca^{2+}-binding proteins that belong to the EF-hand superfamily (*5*). In *S. cerevisiae*, five genes specify small, EF-hand-containing Ca^{2+}-binding proteins: *CMD1*, calmodulin (*6*); *CDC31*, centrin/caltractin (*7*); *CNB1*, calcineurin regulatory subunit (*8*); *MLC1*, myosin light chain (*9*); and, *FRQ1*, frequenin (*10*). The *FRQ1* gene product is particularly interesting because it is a representative of a class of calcium-sensing proteins that is found in metazoans, in cells of the central nervous system, and in other excitable cell types (*11*, *12*). Yeast Frq1 is necessary for cell growth and viability because it regulates the activity and localization of Pik1, a phosphatidylinositol 4-kinase isoform (*10*), an enzyme that has been shown to be essential for secretion in yeast cells (*13*, *14*). Frequenin, the closest homologue of Frq1 in multicellular organisms, may play a similar role in neuronal and neuroendocrine cells (*15*, *16*).

The amino acid sequence of yeast Frq1 (Figure 1) demonstrates its homology to the recoverin branch of the EF-hand superfamily of Ca^{2+}-binding proteins (*17*, *18*). In addition to recoverin, this subgroup of the EF-hand superfamily includes neuronal Ca^{2+} sensors such as neurocalcin,

† This work was supported by NIH Grants EY12347 to J.B.A. and GM21841 to J.T. Kristin B. Hendricks was supported by USPHS Traineeship GM07232, and Inken G. Huttner was supported by a traveling research fellowship from the Daimler-Benz Foundation.

* To whom correspondence should be addressed. Dr. James B. Ames, Center for Advanced Research in Biotechnology, 9600 Gudelsky Drive, Rockville, MD 20850. Phone: (301) 738-6120. Fax: (301) 738-6255. E-mail: james@carb.nist.gov.

‡ University of Maryland Biotechnology Institute.

§ University of California.

Present address: Department of Cell Signaling, DNAX Research Institute, Palo Alto, CA 94304.

10.1021/bi0012890 CCC: $19.00
Published on Web 09/13/2000

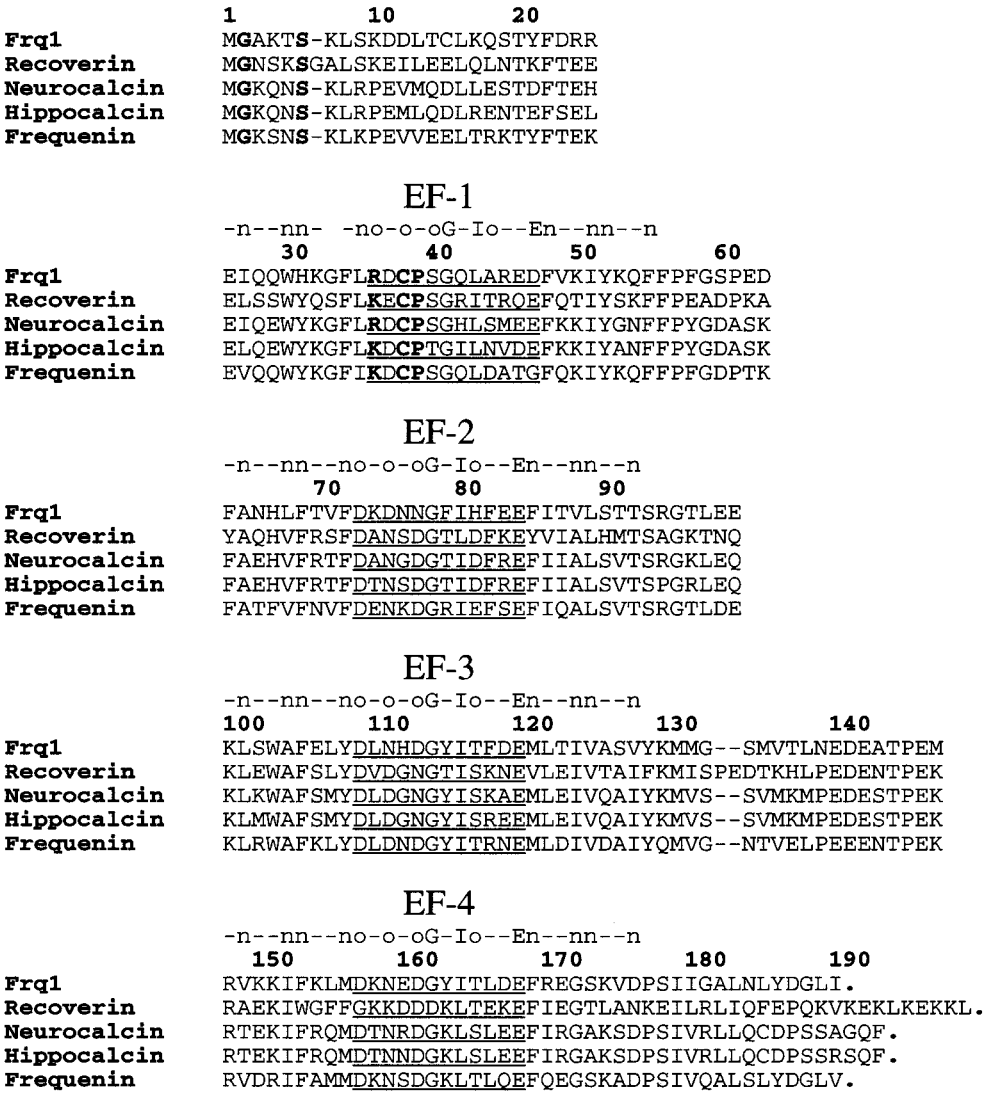

FIGURE 1: Alignment of the primary structure of *S. cerevisiae* Frq1 with various members of the recoverin branch of EF-hand Ca^{2+}-binding proteins. The consensus sequence for the 29-residue EF-hand motif is indicated, where "n" represents any nonpolar residue; "o" represents a residue with an oxygen atom in its side chain (D, N, E, Q, S, or T) that binds to Ca^{2+}; and G, I, and E represents the most highly conserved residues. In each of the four EF-hands, the central Ca^{2+}-binding loop is underlined; residues highlighted in bold in EF-1 prevent Ca^{2+}-binding. The consensus sequence for N-myristoylation at the amino-terminus is also highlighted in boldface. Swiss Protein Database accession numbers are Q06389 (Frq1), P21457 (bovine recoverin), P29554 (bovine neurocalcin), P32076 (rat hippocalcin), and P37236 (*Drosophila* frequenin).

hippocalcin, and frequenin. All members of this group are N-myristoylated and possess four EF-hands, although the first EF-hand motif (EF-1) contains substitutions that prevent Ca^{2+} binding at this site (Figure 1). In recoverin, substitutions in EF-4 also prevent Ca^{2+} binding, and hence only EF-2 and EF-3 are functional (*19*). Frq1 possesses the degenerate EF-1 and three other canonical EF-hand motifs (EF-2, EF-3, and EF-4), is able to bind Ca^{2+}, and is N-myristoylated in vivo (*10*). Frq1 shares 60% identity with frequenin and less similarity (39% identity) with recoverin; correspondingly, expression of frog frequenin, but not bovine recoverin, was able to restore viability to *frq1*Δ yeast cells (*10*).

The three-dimensional structures of the myristoylated and unmyristoylated forms of recoverin in both their Ca^{2+}-free and Ca^{2+}-bound states have been determined by X-ray crystallography (*20*) and nuclear magnetic resonance (NMR) spectroscopy (*21*, *22*). A striking feature of these structures is a large Ca^{2+}-induced conformational change. In the Ca^{2+}-free state, the N-myristoyl group is buried and not exposed to solvent. Binding of Ca^{2+} to recoverin leads, first, to extrusion of its myristoyl group and, second, to a large rotation of the two domains of the protein relative to each other. The Ca^{2+}-induced exposure of the myristoyl group, termed the calcium-myristoyl switch (*19*, *23*), enables Ca^{2+}-bound recoverin to bind to membranes (*24*, *25*).

Given the similarities and differences between Frq1, as a representative frequenin, and recoverin, it was of interest to determine its Ca^{2+}-binding properties, whether it also displays the characteristics of a Ca^{2+}-dependent myristoyl switch protein, and how Ca^{2+}-induced conformation changes contribute to the ability of the protein to associate with membranes. Here we report studies using NMR spectroscopy, fluorescence spectroscopy, equilibrium Ca^{2+}-binding measurements, and subcellular fractionation to analyze the conformational changes in Frq1 due to N-myristoylation and induced by Ca^{2+} binding. Our results suggest that, despite their overall similarity, there are significant differences between Frq1 and recoverin in the effects of Ca^{2+}-binding, which may have important biological implications for the function of frequenins.

EXPERIMENTAL PROCEDURES

Protein Preparation. To prepare unmyristoylated Frq1 and myristoylated Frq1 (myr-Frq1) uniformly labeled with nitrogen-15 and/or carbon-13, Frq1 tagged with a C-terminal $(His)_6$ tract was expressed in *Escherichia coli* strain BL21-(DE3) carrying a derivative of the pET23d vector (Novagen) harboring the *FRQ1* coding sequence, constructed as previously described (*10*), or in the same strain coexpressing a yeast N-myristoyltransferase (*26*), grown in M9 minimal medium containing [^{15}N]NH_4Cl and [$^{13}C_6$]glucose, according to well-established procedures (*27*−*29*). For myr-Frq1, [$^{13}C_{14}$]-myristate (5 mg/L) was added to the medium 0.5 h before induction of protein expression. Labeled Frq1 and myr-Frq1 were purified from the soluble fraction of bacterial cell lysates using Ni^{2+}-chelate affinity chromatography on a nitrilotriacetate-resin (Qiagen), according to the manufacturer's instructions. Peak fractions were then applied to an anion-exchange column (50 mL bed, DEAE-Sepharose, Pharmacia) equilibrated in buffer A (2 mM $CaCl_2$, 20 mM imidazole, pH 6.2) and eluted with a linear salt gradient (0 to 0.5 M KCl) at flow rate of 2 mL min^{-1} over the course of 90 min. Peak fractions were concentrated to 5 mL and subjected to size-exclusion chromatography (Sephacryl S-100, Pharmacia) in buffer B (1 mM dithiothreitol, 2 mM $CaCl_2$, 50 mM HEPES,[1] pH 7.4). Final purity was greater than 98%, as judged by SDS−PAGE. For myr-Frq1, electrospray-ionization mass spectrometry indicated that at least 70−80% of the protein was properly modified.

NMR Spectroscopy. Samples for NMR analysis were prepared by dissolving ^{15}N-labeled or ^{13}C/^{15}N-labeled Frq1 or myr-Frq (1 mM) in 0.5 mL of a 95% H_2O/5% [^{2}H] H_2O solution containing 10 mM [$^2H_2$] imidazole (pH 7.2), 10 mM [$^2H_{10}$] dithiothreitol, 20 mM [$^2H_{28}$] octyl-β-D-glucopyranoside (octyl-glucoside), and either 1 mM EDTA (Ca^{2+}-free) or 5 mM $CaCl_2$ (Ca^{2+}-bound). All NMR experiments were performed at 35 °C on a Bruker DRX-500 or DRX-600 spectrometer equipped with a four-channel interface and a triple-resonance probe with triple-axis pulsed field gradients. The ^{15}N-^{1}H HSQC spectra (see Figure 4) were recorded on a sample of ^{15}N-labeled Frq1 (in 95% H_2O, 5% ^2H_2O). The number of complex points and acquisition times were 256, 180 ms [^{15}N (F_1)] and 512, 64 ms [^{1}H (F_2)]. The ^{13}C-^{1}H HSQC spectra (see Figure 7) were recorded on a sample of unlabeled Frq1 protein containing a uniformly ^{13}C-labeled myristoyl group (*22*). All triple-resonance experiments were performed as described previously (*30*) on a sample of ^{13}C/^{15}N-labeled Frq1 (in 95% H_2O, 5% ^2H_2O) with the following number of complex points and acquisition times: HNCO {^{15}N (F_1) 32, 23.7 ms; ^{13}CO (F_2) 64, 42.7 ms; ^{1}H (F_3) 512, 64 ms}; HNCACB {^{15}N (F_1) 32, 23.7 ms; ^{13}C (F_2) 48, 6.3 ms; ^{1}H (F_3) 512, 64 ms}; CBCACONNH {^{15}N (F_1) 32, 23.7 ms; ^{13}C (F_2) 48, 6.3 ms; ^{1}H (F_3) 512, 64 ms}; CBCACOCAHA {^{13}C (F_1) 52, 6.8 ms, ^{13}CO (F_2) 64, 42 ms, ^{1}H (F_3) 384, 64 ms}; and, HBHACONNH {^{15}N (F_1) 32, 23.7 ms, $^1H_{ab}$ (F_2) 64, 21 ms, ^{1}H (F_3) 512, 64 ms}. The triple-resonance spectra were processed and analyzed as described previously (*30*).

Structure Calculation. Backbone and side chain NMR resonances of Frq1 were assigned as described previously (*30*). Structure calculations for Frq1 were performed using the YASAP protocol within X-PLOR (*31*, *32*), as described previously (*33*). A total of 1050 interproton distance constraints was obtained as described (*30*) by analysis of ^{13}C-edited and ^{15}N-edited NOESY−HSQC spectra (120 ms mixing time) of ^{13}C,^{15}N-labeled Frq1. Additional distance constraints for conserved amino-terminal residues were derived from NOESY−HSQC spectra of Ca^{2+}-bound recoverin (*19*). In addition to the NOE-derived distance constraints, the following additional constraints were included in the structure calculation: 18 distance constraints involving Ca^{2+} bound to loop residues 1, 3, 5, 7, and 12 in each EF-hand motif (EF-2, EF-3, and EF-4); 140 distance constraints for 70 hydrogen bonds; and 300 dihedral angle constraints. Fifty independent structures were calculated, and the 20 structures of lowest energy were selected. The average total and experimental distance energies are 4125 and 72 kcal mol^{-1}. The average root-mean-square (RMS) deviations from an idealized geometry for bonds and angles are 0.0074 Å and 2.04°. None of the distance and angle constraints were violated by more than 0.40 Å or 4°, respectively.

Fluorescence Spectroscopy. The effect of Ca^{2+} on the intrinsic tryptophan fluorescence emission of Frq1, excited at 280 nm, was measured (at 300−420 nm) using a SPEX fluorimeter. Calcium titrations (see Figure 3) were performed with 2 μM Frq1 in 2 mL of 50 mM HEPES (pH 7.5), 0.1 M KCl, 1 mM dithiothreitol at 25 °C at free Ca^{2+} concentrations (30 nM to 1 μM) set using a Ca^{2+}-EGTA buffering system. The free Ca^{2+} concentration was calculated based on the total amounts of Ca^{2+} and EGTA present using a computer algorithm (*34*). The protein samples initially contained an equal molar ratio of total Ca^{2+} and EGTA (1 mM); the concentration of free Ca^{2+} was sequentially reduced by adding aliquots of 0.1 M EGTA. The calculated free Ca^{2+} concentrations agreed closely with direct measurements of Ca^{2+} concentration made using the fluorescent indicator dyes, fluo-3 and rhod-2 (Molecular Probes, Eugene, OR), which have K_d of 0.4 and 1.0 μM, respectively (*38*), or using a Ca^{2+}-selective electrode (Orion, Boston, MA), when the Ca^{2+} concentration exceeded 1 μM.

Binding of $^{45}Ca^{2+}$. $^{45}Ca^{2+}$ binding to Frq1 was measured as the protein-bound radioactivity retained after ultrafiltration using a procedure (*35*) based on the original method of Paulus (*36*). Briefly, Frq1 (10, 50, and 100 μM protein in the presence and absence of 20 mM octyl glucoside) dissolved in 1.5 mL of 50 mM HEPES (pH 7.5), 0.1 M KCl, and 1 mM dithiothreitol was placed in the sample compartment of a Centricon-10 concentrator (molecular mass cutoff, 10 kDa), and 20 μL of 0.25 mM $^{45}CaCl_2$ solution (1 μCi) was added. The sample was subjected to centrifugation (at 2000 rpm) in a tabletop centrifuge (Beckman model TJ-6) at room temperature for 30 s, forming 20 μL of filtrate. The radioactivity in the filtrate (free Ca^{2+}) and the radioactivity in an equal volume of the protein sample (total Ca^{2+}) were determined by liquid scintillation counting. Successive additions of nonradioactive Ca^{2+} were made to the protein sample, and the above centrifugation procedure was repeated. After each addition of nonradioactive ligand, the free Ca^{2+}

[1] Abbreviations: EDTA, *N*,*N*,*N*′,*N*′-ethylenediaminetetraacetic acid; EGTA, ethylene glycol-bis(b-aminoethyl ether)-*N*,*N*,*N*′,*N*′-tetraacetic acid; HEPES, (*N*-{2-hydroxyethyl}piperazine-*N*′-{2-ethanesulfonic acid}); HMQC, heteronuclear multiple quantum coherence; HSQC, heteronuclear single quantum coherence; NOESY, nuclear Overhauser effect spectroscopy; RMS, root-mean-square; SDS−PAGE, sodium dodecyl sulfate−polyacrylamide gel electrophoresis.

concentration was calculated from the measured radioactivity as follows:

$$Ca^{2+}_{free} = \frac{r_a}{r_b} Ca^{2+}_{total} \quad (1)$$

where r_a is the radioactivity of the filtrate, r_b is radioactivity of protein sample, and Ca^{2+}_{total} is the total Ca^{2+} concentration. The concentration of Ca^{2+} bound to protein is therefore

$$Ca^{2+}_{bound} = Ca^{2+}_{total} - Ca^{2+}_{free} \quad (2)$$

Hence, the fractional saturation can be defined as

$$Y = \frac{Ca^{2+}_{bound}}{nP_{tot}} = \frac{\{Ca^{2+}_{free}\}^a}{\{Ca^{2+}_{free}\}^a + \{K_d\}^a} \quad (3)$$

where P_{tot} is the total protein concentration in the system, n is the number of bound Ca^{2+}, a is the Hill coefficient, and K_d is the apparent dissociation constant.

Subcellular Fractionation. To assess the effect of the presence of Ca^{2+} and/or the N-myristoyl group on the ability of Frq1 to associate with membranes, the distribution of Frq1 in cell-free extracts of yeast cells expressing wild-type Frq1 (strain YKBH5) or a nonmyristoylated mutant, Frq1(G2A) (strain YKBH6) (*10*), was examined as follows. After growth, cells were first rinsed in buffer [3 mM dithiothreitol, 1 mM phenylmethanesulfonylfluoride, 1 μg/mL leupeptin, 1 μg/mL pepstatin A, and 50 mM Tris-HCl (pH 7.5)] containing either 1 mM $CaCl_2$ or 10 mM EDTA plus 10 mM EGTA. The washed cells were then lysed, as described in detail elsewhere (*10*), in the same buffer containing either 200 μM $CaCl_2$ or 5 mM EDTA plus 5 mM EGTA. Unlysed cells and large cellular debris were removed by centrifugation at 500*g* for 5 min at 4 °C in the SS-34 rotor of a refrigerated preparative centrifuge (Dupont/Sorvall). Protein concentration of the clarified extracts was determined, and each extract was adjusted with its respective buffer to a final concentration of 1.0−1.5 mg/mL. After reserving a sample (5 μL) of each lysate, another sample (100 μL) was subjected to centrifugation for 30 min at 10000*g* in the same rotor and centrifuge. The resulting supernatant fraction of each extract was transferred to a fresh tube, after reserving a sample (10 μL) for analysis, and subjected to centrifugation for 30 min at 60000*g* in a tabletop ultracentrifuge (TL-100, Beckman) at 4 °C. The pellet of the 10000*g* sedimentation was resuspended in an equal volume of the appropriate lysis buffer. The supernatant fraction of the 60000*g* sedimentation was transferred to a fresh tube, after reserving a sample (10 μL) for analysis, and subjected to centrifugation for 30 min at 100000*g* in the tabletop ultracentrifuge. The pellet of the 60000*g* sedimentation was resuspended in an equal volume of the appropriate lysis buffer. The final supernatant fraction was withdrawn, and the final pellet was resuspended in an equal volume of the appropriate lysis buffer. Equivalent volumes of the original clarified lysate and the supernatant fractions and resuspended pellets of the 10000*g*, 60000*g*, and 100000*g* sedimentations were analyzed by SDS−PAGE and immunoblotting with specific rabbit polyclonal anti-Frq1 antibodies, as described in detail elsewhere (*10*).

RESULTS

Equilibrium Ca^{2+}-Binding Measurements. Frq1 contains four EF-hand Ca^{2+}-binding motifs (*10*). However, like other members of the recoverin-related group (Figure 1), EF-1 of Frq1 contains substitutions (Arg36, Cys38, and Pro 39) that disrupt the structure of this binding loop and prevent Ca^{2+} binding to EF-1, as seen in the crystal structures of both recoverin and neurocalcin (*20*, *37*). At least in recoverin, disabling of Ca^{2+} binding to EF-1 seems to be important for its calcium-myristoyl switch mechanism because residues of EF-1 in Ca^{2+}-free recoverin make physical contact with the N-myristoyl group (*19*). Likewise, the presence of residues that potentially disable Ca^{2+} binding to its EF-1 suggests that Frq1 may possess a similar calcium-myristoyl switch mechanism. In contrast to recoverin, in which EF-4 is also disabled by substitutions incompatible with Ca^{2+} binding, the remaining motifs in Frq1 (EF-2, EF-3, and EF-4) are good matches to the consensus and should bind Ca^{2+}. To determine if these predictions are correct and to assess how many ions bind to Frq1 at saturation, direct measurements of Ca^{2+} binding were performed.

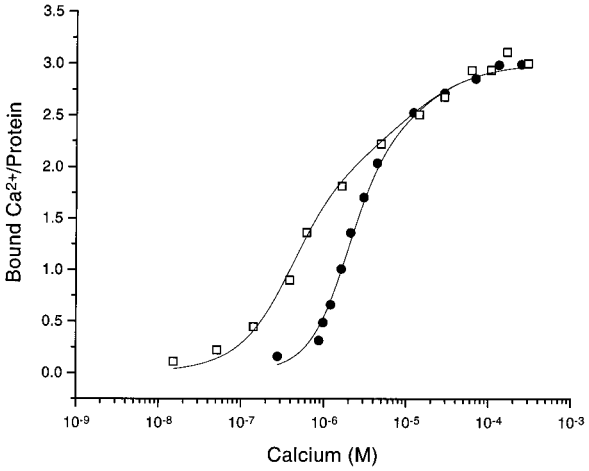

FIGURE 2: Equilibrium Ca^{2+} binding to Frq1 and myr-Frq1. Titrations of $^{45}Ca^{2+}$ binding to Frq1 (open squares) and to myr-Frq1 (filled circles) were conducted using an ultrafiltration method, as described in Experimental Procedures. Number of ions bound per molecule of protein is plotted versus the free calcium concentration. Solid lines represent the best fit to a concerted model for allosteric transition using the parameters as defined in the text: K_{EF2} = 10 μM, $K_{EF3} = K_{EF4}$ = 0.4 μM, c = 0.01, and L = 20 (myristoylated) and 0.02 (unmyristoylated). The measured dissociation constants were not affected by the presence or absence of detergent and were independent of protein concentration, in the range from 10 to 100 μM (data not shown).

Equilibrium measurements of $^{45}Ca^{2+}$ binding were conducted on Frq1 and myr-Frq1 (Figure 2). At saturation, three Ca^{2+} bind to each form of the protein, consistent with the view that EF-1 is disabled, whereas EF-2, EF-3, and EF-4 are functional. The fractional saturation (Y), which can be obtained from the same data, can be represented by the Hill equation:

$$Y = \frac{[Ca^{2+}]^a}{[Ca^{2+}]^a + K_d^a} \quad (4)$$

where $[Ca^{2+}]$ is the free Ca^{2+} concentration, K_d is the apparent dissociation constant, and a denotes the Hill coefficient. The slope of the titration for unmodified Frq1 suggests rather heterogeneous binding of Ca^{2+} (average $K_d$app = 700 nM and a = 0.79). Likewise, a Scatchard plot of the same data is biphasic (not shown). This heterogeneity

indicates that Frq1 contains multiple Ca^{2+}-binding sites with distinct intrinsic affinities.

Given three different Ca^{2+}-binding sites, a total of 12 different binding equilibria are expected for Frq1:

$$P_{000} + Ca^{2+} \leftrightarrow P_{001} \ldots\ldots K_{D1} = \frac{P_{000}[Ca^{2+}]}{P_{001}}$$

$$P_{000} + Ca^{2+} \leftrightarrow P_{010} \ldots\ldots K_{D2} = \frac{P_{000}[Ca^{2+}]}{P_{010}}$$

$$P_{000} + Ca^{2+} \leftrightarrow P_{100} \ldots\ldots K_{D3} = \frac{P_{000}[Ca^{2+}]}{P_{100}}$$

$$P_{001} + Ca^{2+} \leftrightarrow P_{011} \ldots\ldots K_{D4} = \frac{P_{001}[Ca^{2+}]}{P_{011}}$$

$$P_{001} + Ca^{2+} \leftrightarrow P_{101} \ldots\ldots K_{D5} = \frac{P_{001}[Ca^{2+}]}{P_{101}}$$

$$P_{010} + Ca^{2+} \leftrightarrow P_{011} \ldots\ldots K_{D6} = \frac{P_{010}[Ca^{2+}]}{P_{011}}$$

$$P_{010} + Ca^{2+} \leftrightarrow P_{110} \ldots\ldots K_{D7} = \frac{P_{010}[Ca^{2+}]}{P_{110}}$$

$$P_{100} + Ca^{2+} \leftrightarrow P_{101} \ldots\ldots K_{D8} = \frac{P_{100}[Ca^{2+}]}{P_{101}}$$

$$P_{100} + Ca^{2+} \leftrightarrow P_{110} \ldots\ldots K_{D9} = \frac{P_{100}[Ca^{2+}]}{P_{110}}$$

$$P_{011} + Ca^{2+} \leftrightarrow P_{111} \ldots\ldots K_{D10} = \frac{P_{011}[Ca^{2+}]}{P_{111}}$$

$$P_{101} + Ca^{2+} \leftrightarrow P_{111} \ldots\ldots K_{D11} = \frac{P_{101}[Ca^{2+}]}{P_{111}}$$

$$P_{110} + Ca^{2+} \leftrightarrow P_{111} \ldots\ldots K_{D12} = \frac{P_{110}[Ca^{2+}]}{P_{111}}$$

where P_{ijk} denotes occupancy of sites *i*, *j*, and *k*, and the K_D values are the corresponding dissociation constants. If the sites are independent (i.e., $K_{D1} = K_{D6} = K_{D8} = K_{D12} = K_{EF4}$ and $K_{D2} = K_{D4} = K_{D9} = K_{D11} = K_{EF3}$ and $K_{D3} = K_{D5} = K_{D7} = K_{D10} = K_{EF2}$), then the fractional saturation expression simplifies to

$$Y = 0.33\left(\frac{[Ca^{2+}]}{[Ca^{2+}] + K_{EF2}} + \frac{[Ca^{2+}]}{[Ca^{2+}] + K_{EF3}} + \frac{[Ca^{2+}]}{[Ca^{2+}] + K_{EF4}}\right) \quad (5)$$

where K_{EF2} represents the dissociation constant for EF-2, etc. In fact, the binding data for Frq1 are fit well by this equation if the corresponding K_d values are set as $K_{EF3} = K_{EF4} = 0.4$ μM and $K_{EF2} = 10$ μM, assuming that EF-2 represents the site with the weaker affinity. In recoverin, EF-2 was shown to bind Ca^{2+} with much lower affinity ($K_{EF2} = 7$ μM) than EF-3 ($K_{EF3} = 0.1$ μM) based on the X-ray structure (reviewed in ref *38*) and site-directed mutagenesis studies (*39*).

In comparison to unmodified Frq1, the titration for myr-Frq1 exhibited a steeper Ca^{2+} dependence with a somewhat lower apparent affinity (Figure 2). The Hill equation for the data for myr-Frq1 are best fit by $K_d$app = 3 μM and a = 1.25. The positive cooperativity of binding and the lower apparent affinity in myr-Frq1 can be rationalized using a concerted (two-state) model for Ca^{2+}-induced allosteric transitions, which has been used previously to explain cooperative Ca^{2+} binding to myristoylated recoverin (*40*). In this model, two conformational states of the protein are postulated, "T" and "R":

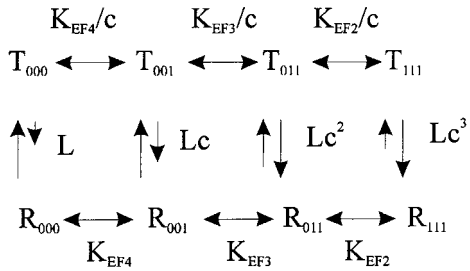

where K_{EF2}, K_{EF3}, and K_{EF4} denote the dissociation constants of the three EF-hands in the R state. An assumption is made that the global transition from R to T changes the binding constant of all three sites by the same factor, *c*. *L* is the intrinsic equilibrium constant for the allosteric transition in the absence of ligands, i.e., the T_{000}/R_{000} ratio. According to this model, the equilibria are given by

$$K_{EF4} = \frac{[Ca^{2+}]R_{000}}{R_{001}} = \frac{c[Ca^{2+}]T_{000}}{T_{001}} \quad (6)$$

$$K_{EF3} = \frac{[Ca^{2+}]R_{001}}{R_{011}} = \frac{c[Ca^{2+}]T_{001}}{T_{011}} \quad (7)$$

$$K_{EF2} = \frac{[Ca^{2+}]R_{011}}{R_{111}} = \frac{c[Ca^{2+}]T_{011}}{T_{111}} \quad (8)$$

$$L = \frac{T_{000}}{R_{000}} = \frac{T_{001}}{cR_{001}} = \frac{T_{011}}{c^2R_{011}} = \frac{T_{111}}{c^3R_{111}} \quad (9)$$

where R_{ijk} and T_{ijk} represent Frq1 in the R and T states, and the subscripts *i*, *j*, and *k* denote the occupancy of EF-2, EF-3, and EF-4, respectively. The fractional saturation can thus be reduced to the expression:

$$Y = \left\{\beta\frac{[Ca^{2+}]}{K_{EF4}} + 2\gamma\frac{[Ca^{2+}]^2}{K_{EF4}K_{EF3}} + 3\delta\frac{[Ca^{2+}]^3}{K_{EF2}K_{EF3}K_{EF4}}\right\} \Big/ \left\{1 + L^{-1} + \beta\frac{[Ca^{2+}]}{K_{EF4}} + \gamma\frac{[Ca^{2+}]^2}{K_{EF4}K_{EF3}} + \delta\frac{[Ca^{2+}]^3}{K_{EF2}K_{EF3}K_{EF4}}\right\} \quad (10)$$

where $\beta = c + L^{-1}$, $\gamma = c^2 + L^{-1}$, and $\delta = c^3 + L^{-1}$. The binding data observed for myr-Frq1 are well fit by this model using the dissociation constants determined for unmodified Frq1 ($K_{EF2} = 10$ μM and $K_{EF3} = K_{EF4} = 0.4$ μM). *L* is calculated to be 21 for myr-Frq1 and <0.02 for Frq1. The parameter *c* is not well-defined by the binding data and was

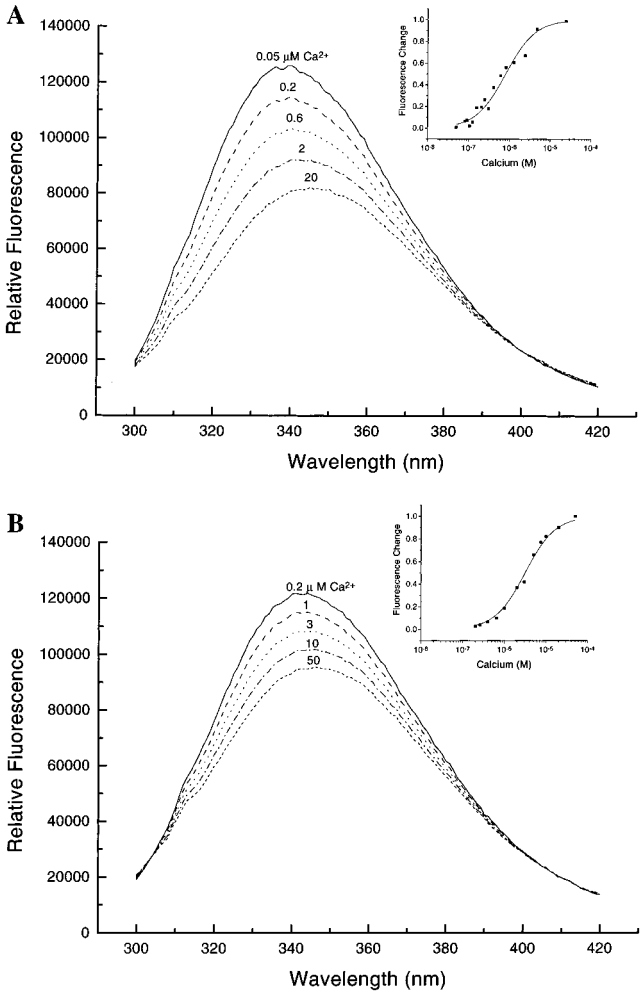

FIGURE 3: Effect of Ca^{2+} on intrinsic tryptophan fluorescence of Frq1. Fluorescence emission spectra for Frq1 (A) and myr-Frq1 (B) were recorded at the indicated Ca^{2+} concentrations. Inset: the change in fluorescence intensity at 340 nm is plotted as a function of the free Ca^{2+} concentration.

estimated to be less than 0.01. Both the observed cooperative Ca^{2+} binding by myr-Frq1 and the apparent uncooperative Ca^{2+} binding by unmodified Frq1 can be modeled simply by varying L (while keeping all the other parameters fixed). Viewed in this fashion, the myristoyl group induces cooperative Ca^{2+} binding because it favors the T state ($L = 21$), and conversely, for unmodified Frq1, the R state is more stable ($L < 0.02$). Hence, one interpretation of the function of the myristoyl group in Frq1 is that it serves as a built-in allosteric effector, as was previously suggested for recoverin (*40*).

Fluorescence Spectroscopy to Monitor Ca^{2+}-Induced Conformational Changes. The above analysis of Ca^{2+} binding to Frq1 suggests two conformational states of the protein, T and R. As one means to demonstrate that Frq1 actually undergoes Ca^{2+}-induced structural transitions, we examined the effect of Ca^{2+} on the intrinsic tryptophan fluorescence of Frq1, which contains two tryptophan residues (Trp30 and Trp103). The fluorescence emission of tryptophan is very sensitive to its surrounding chemical environment and, hence, provides an effective probe of structural changes in a protein (*41*). In the absence of Ca^{2+}, the fluorescence emission spectra of unmodified Frq1 (Figure 3, panel A) and myr-Frq1 (Figure 3, panel B) each had a maximum at 340 nm and were very similar, suggesting that N-myristoylation by itself does not alter significantly the overall structure of the protein. Upon Ca^{2+} binding to either Frq1 or myr-Frq1, the emission maximum shifted to longer wavelength (by 4 nm), and at saturation, the emission intensity decreased by 35%. On the basis of first principles (*41*), these changes suggest that one or both Trp residues shift into a more polar chemical environment when the protein is in its Ca^{2+}-bound state relative to its Ca^{2+}-free state. These changes in tryptophan fluorescence may reflect global conformational changes or may report primarily local changes in the environment around Trp103 that occur upon Ca^{2+} binding because Trp103 is located within the α-helix that leads into the Ca^{2+}-binding loop of EF-3 (see below). The change in fluorescence intensity plotted against Ca^{2+} concentration (Figure 3, insets) provides another measure of the Ca^{2+} affinity of the protein. The midpoint of these titrations occurs at Ca^{2+} concentrations near 700 nM (unmodified Frq1) and 3 μM (myr-Frq1), in excellent agreement with the apparent K_d values obtained from the equilibrium Ca^{2+}-binding measurements (Figure 2). Hence, conformational changes induced in Frq1 upon Ca^{2+} binding are likely to be concerted.

Structural Studies using NMR. Conformational changes in Frq1 resulting from Ca^{2+} binding were also monitored by nuclear magnetic resonance (NMR) spectroscopy. Two-dimensional NMR spectra (^1H-^{15}N HSQC) of uniformly ^{15}N-labeled Ca^{2+}-free and Ca^{2+}-bound forms of Frq1 and myr-Frq1 were collected (Figure 4). Peaks in each spectrum represent main chain and side chain amide protons that serve as fingerprints of overall conformation. To derive three-dimensional structure from NMR data, each peak in the spectrum must first be assigned to a particular residue in the amino acid sequence.

The NMR spectrum of Ca^{2+}-free Frq1 exhibited highly congested and poorly resolved peaks (Figure 4, panel A), making it very difficult, if not impossible, to make sequence-specific assignments. The number of observed peaks (140) was far less than expected (189 main chain + 70 side chain = 259 amide protons). Many of the peaks were not detected apparently because they were severely broad and weak. The variable range of peak intensities suggested that some of the peaks might be broadened due to self-association of Frq1 molecules in concentrated solution (1 mM protein concentration) required for NMR. Indeed, dynamic light-scattering measurements performed on the solutions used for NMR confirmed that the Ca^{2+}-free Frq1 samples contained a broad distribution of multimeric species with an average molecular mass of ~64 kDa (data not shown), consistent with formation of at least a dimer and very likely higher aggregates. Interestingly, during the final step of purification (size-exclusion chromatography on Sephacryl S-100), Frq1 eluted as a monomer (data not shown), suggesting that Frq1−Frq1 association is low-affinity and has a fast off-rate. Adding detergent (octyl-glucoside) substantially improved the solubility of Frq1 and reduced aggregation significantly. Also, the presence of this detergent sharpened the line widths but did not significantly change the peak positions in the NMR spectra. Hence, octyl-glucoside did not appear to affect the structure of the protein. Therefore, all of the NMR experiments reported here were performed on samples of Frq1 that contained 20 mM octyl-glucoside.

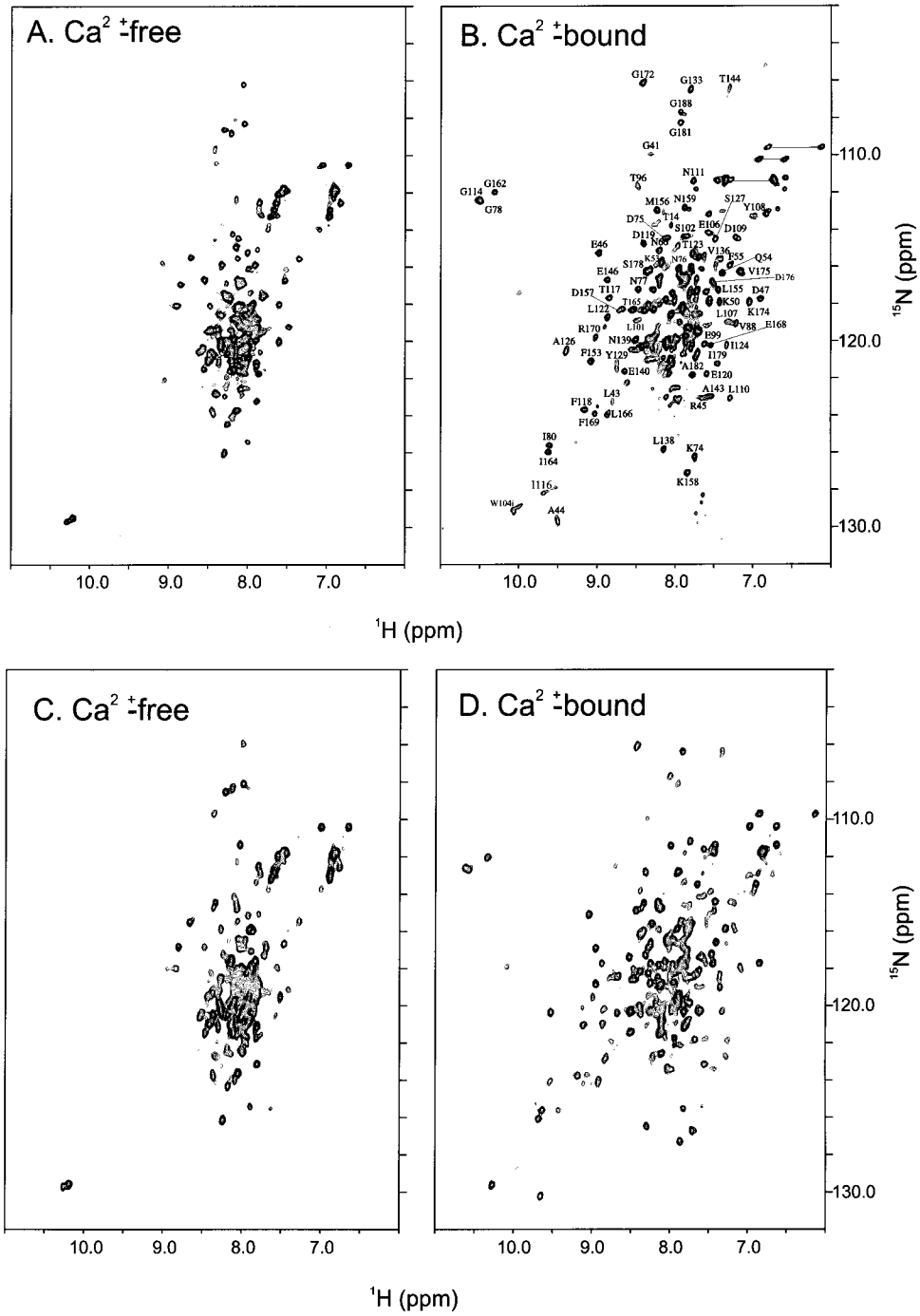

FIGURE 4: Two-dimensional ^{15}N-^{1}H HSQC NMR spectra of Frq1. Two-dimensional ^{15}N-^{1}H HSQC NMR spectra for Ca^{2+}-free Frq1 (A), Ca^{2+}-bound Frq1 (B), Ca^{2+}-free myr-Frq1 (C), and Ca^{2+}-bound myr-Frq1 (D), each uniformly labeled with nitrogen-15, were recorded at 600-MHz ^{1}H frequency in the presence of 20 mM octyl-glucoside. Peaks corresponding to the $-NH_2$ groups of the side chain amides of Gln and Asn residues are connected by dotted lines. Sequence-specific assignments are indicated for Ca^{2+}-bound unmodified Frq1 and have been deposited into the BioMagResBank Repository (accession no. 4798).

In contrast to the Ca^{2+}-free form, the NMR spectrum of Ca^{2+}-bound Frq1, exhibited many sharp and well-resolved peaks (Figure 4, panel B). The striking Ca^{2+}-induced spectral differences are consistent with large Ca^{2+}-induced structural changes in the protein. The intensity of the peaks characteristic of the Ca^{2+}-bound form saturated upon addition of 3 molar equiv of Ca^{2+} to the sample, in good agreement with the stoichiometry of Ca^{2+} binding determined from the equilibrium Ca^{2+}-binding experiments (Figure 2). The total number of observable peaks in the spectrum of Ca^{2+}-bound Frq1 is somewhat fewer than expected (180 vs 259), presumably because some of the resonances have extremely weak intensity and therefore escaped detection. Again, the wide range of peak intensities observed was suggestive of the formation of multimeric species. Dynamic light-scattering studies performed on the concentrated sample of Ca^{2+}-bound Frq1 indicated a relatively narrow distribution of species with average molecular mass of ~58 kDa (data not shown), suggesting that, in its Ca^{2+}-bound form and under the conditions of the NMR measurements (1 mM protein concentration), Frq1 forms mainly a dimeric species.

The two-dimensional (^{1}H-^{15}N HSQC) NMR spectra of myr-Frq1 in the absence and presence of Ca^{2+} (Figure 4, panels C and D) are almost identical to those for unmodified

Frq1 described above (Figure 4, panels A and B). Hence, the presence of the N-myristoyl group does not appear to affect the structure of Frq1, in contrast to the structural changes in recoverin that depend on its N-myristoyl group (*23*). The similarities in the spectra of Frq1 and myr-Frq1 suggests that the fatty acyl chain may be exposed to solvent and, hence, not interacting significantly with the protein. A solvent-exposed N-myristoyl group may help explain the high degree of aggregation and low solubility of myr-Frq1 observed in concentrated solution in the absence of detergent.

Secondary Structure of Frq1 by NMR. The strong and well-resolved peaks observed in the spectrum of Ca^{2+}-bound Frq1 (Figure 4, panel B) made it feasible to determine sequence-specific assignments. Triple resonance experiments correlating ^{15}N, ^{13}C, and ^{1}H were performed and analyzed to make the assignments, using procedures described previously (*30*). Over 90% of the backbone resonances from residues in the carboxy-terminal half of the protein (Lys100 to Ile190) were assigned (Figure 4, panel B). In addition, 20% of the resonances from residues in the amino-terminal half of the protein were assigned. All of these assignments have been deposited into the BioMagResBank Repository (accession no. 4798). The remaining unassigned residues exhibited extremely weak NMR signals, most likely due to chemical exchange broadening perhaps caused by the participation of these groups in the protein−protein interactions responsible for dimer formation.

The sequence-specific assignments (Figure 4, panel B) enabled us to analyze characteristic NMR resonances (C_α, H_α, and C′) and determine secondary structure in Ca^{2+}-bound Frq1 (Figure 5). The chemical shift index (see ref *42* for detailed description of the chemical shift index), $^3J_{NH\alpha}$ coupling constants, and nuclear Overhauser effect (NOE) connectivity patterns for each residue were analyzed and provided a measure of the overall secondary structure. Small $^3J_{NH\alpha}$ coupling constants (<5 Hz), strong NOE connectivities [NN(i,i+1) and αN(i,i+3)], and positive chemical shift index are characteristic of residues in an α-helix. Conversely, large $^3J_{NH\alpha}$ coupling constants (>8 Hz), strong αN(i,i+1) and weak NN(i,i+1) NOE connectivities, and negative chemical shift index are characteristic of residues in a *β*-strand.

The results of this analysis of the secondary structure of Frq1 are summarized in Figure 5. The conformation of the first 41 residues of Frq1 could not be determined because the NMR resonances of these residues were unassigned due to their very weak NMR intensities. Consistent with the overall architecture of EF-hand motifs, the EF-1 region of Frq1 (Glu26−Phe55) contains a short *β*-strand (Gln42−Arg45) and an α-helix (Glu46−Phe55). Similarly, in the EF-2 region (Phe64−Thr92), a *β*-strand (Phe79−Val88) and nine-residue α-helix (Phe82−Leu89) were observed. In the C-terminal half of the protein (Lys100−Ile190), the observed secondary structure matches very well the canonical helix−loop−helix structure of other EF-hand motifs. The EF-3 region of Frq1 contains a 10-residue α-helix (Leu101−Tyr108) followed by a six-residue turn (Asp109−Gly114), a short *β*-strand (Tyr115−Thr117), and a 10-residue α-helix (Phe118−Tyr129). The residues between EF-3 and EF-4 (Lys130−Pro145) assume "random-coil" geometry. The EF-4 segment of Frq1 contains an 11-residue α-helix (Glu146−Met156), a six-residue turn (Asp157−Gly162), a short *β*-strand (Tyr163−Thr165), and a 10-residue α-helix

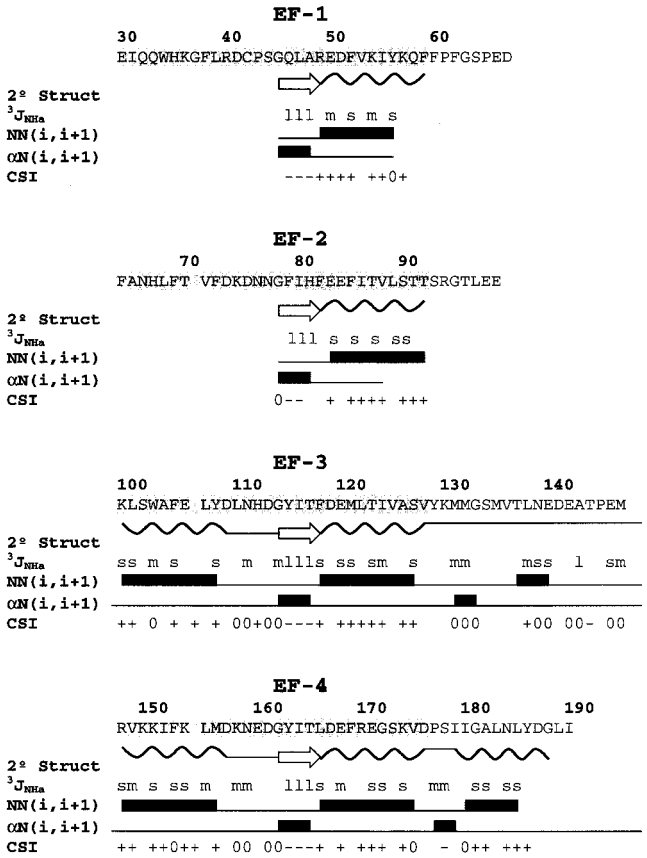

FIGURE 5: Schematic diagram of the secondary structure of Frq1. This figure summarizes the NMR data—sequential and medium-range NOEs involving NH and Hα resonances, $^3J_{NH\alpha}$ coupling constants, and chemical shift index (*42*) calculated from secondary shifts of $^1H_\alpha$, $^{13}C_\alpha$, and ^{13}CO of Ca^{2+}-bound Frq1—and its implications for deducing secondary structure. Secondary structure is depicted by white arrows (*β*-strands) and wavy lines (α-helices). The $^3J_{NH\alpha}$ coupling constants are denoted as "large" (l; >8 Hz), "medium" (m; 5−8 Hz), and "small" (s; <5 Hz). NOE connectivities [NN(i,i+1) and αN(i,i+1)] are represented as strong, weak, or zero intensity in bar graphs. The chemical shift index of each residue (−1, 0, +1) is represented by a −, 0, or +, respectively. The EF-hands in the sequence are shaded.

(Leu166−Val175). A short C-terminal α-helix (Ile179−Asp187) lies immediately distal to EF-4.

The secondary structure pattern derived for Ca^{2+}-bound Frq1 is nearly identical to the corresponding secondary structure of Ca^{2+}-bound recoverin. In addition, the chemical shifts of backbone resonances from residues conserved between Frq1 and recoverin are nearly identical to those of recoverin. Important long-range NOE interactions between EF-2 and EF-3 (e.g., His67−Ile124 and Leu68−Leu107) and EF-3 and EF-4 (Ile116−Ile164, Leu101−Leu166, and Phe106−Phe169) are seen in the three-dimensional NOESY spectra of Ca^{2+}-bound Frq1 and are consistent with the short distances (<5 Å) observed between the corresponding residues in the structure of Ca^{2+}-bound recoverin (*19*). Taken together, the NMR data obtained for Frq1 strongly suggest that the overall three-dimensional structure of Ca^{2+}-bound Frq1 is very similar to that of Ca^{2+}-bound recoverin.

Three-Dimensional Structure of Frq1 by Homology Modeling. The high degree of primary structure homology between Frq1 and recoverin (Figure 1), and the strong similarities between the NMR spectral signatures of Ca^{2+}-bound Frq1 and Ca^{2+}-bound recoverin discussed immediately

above, suggested that the overall three-dimensional structures of these two proteins may be quite similar. We concluded, therefore, that a reasonable approximation of the three-dimensional structure of Frq1 could be generated by combining structural constraints for the carboxy-terminal region of Ca^{2+}-bound Frq1 (K100−I190) derived from the NMR analysis obtained in this study with structural constraints for residues conserved between the two proteins derived from the known structure of Ca^{2+}-bound recoverin (*19*). The proposed structure derived in this way (Figure 6) represents a more than plausible interpretation of the available NMR data. To calculate this three-dimensional model of Frq1 structure, more than 2000 proton−proton distance relationships (derived from nuclear Overhauser effect data) and more than 300 dihedral angle constraints (derived from *J*-coupling and chemical shift data) were applied using distance geometry and restrained molecular dynamics. Nevertheless, the model should not be misconstrued as a de novo structure determination.

The ensemble of lowest energy structures for Ca^{2+}-bound Frq1 calculated based on the NMR data are shown in Figure 6, panel A; the average structure is depicted as a ribbon diagram in the accompanying panel (Figure 6, panel B). Overall, Frq1 contains two tightly packed domains. Each domain contains a pair of EF-hand motifs: EF-1 and EF-2 interact to form the amino-terminal domain, and EF-3 and EF-4 associate to form the carboxy-terminal domain. The entering helix of EF-2 (residues 62−72) packs against the helices of EF-3 (residues 100−108 and 118−129) at the interface between the two domains, forming a cleft. Additional α-helices are present near the N-terminus (residues 9−16) and C-terminus (residues 179−186). The linker between the two domains is U-shaped, which positions the four EF-hands in a tandem linear array, like that seen previously in the structures of Ca^{2+}-bound recoverin (*23*), neurocalcin (*37*), and GCAP-2 (*43*), and unlike the dumbbell arrangement found in calmodulin (*44*) and troponin C (*45*).

In the structural model of Frq1, three Ca^{2+} are bound (at EF-2, EF-3, and EF-4). Calcium is not bound to EF-1 due to an unfavorable Ca^{2+}-binding geometry, attributable primarily to Pro39 at the fourth position of this binding loop (Figure 1). The three EF-hands occupied by Ca^{2+} adopt the familiar open conformation seen previously in recoverin, calmodulin, and troponin C. An important difference between Frq1 and recoverin can be seen in the structure of EF-4. Ca^{2+} binds to EF-4 in Frq1, whereas this site is disabled in recoverin. In Frq1, residues 1 and 3 of the EF-4 loop (Asp157 and Asn159) contain oxygen atoms in their side chains that can coordinate Ca^{2+}; in contrast, the corresponding residues in recoverin (Gly160 and Lys162) are unable to do so.

NMR Analysis of {^{13}C}Myristate-Labeled Frq1. In addition to the difference between the function of EF-4 in Frq1 and recoverin, another potential difference between these two proteins that could contribute to their different physiological roles is the disposition of the N-terminal myristoyl group. Previously, two-dimensional (^1H-^{13}C HSQC) and three-dimensional (^{13}C-filtered NOESY-HMQC) NMR experiments on samples of unmodified recoverin and recoverin that contained a ^{13}C-labeled myristoyl group were used to selectively probe the chemical environment around the amino-terminal myristoyl group (*22*, *30*). These studies revealed that the covalently attached fatty acyl chain in recoverin is sequestered in a hydrophobic pocket in the Ca^{2+}-free protein (*39*) and that binding of Ca^{2+} leads to conformational changes that extrude the N-myristoyl group into solvent.

Similar NMR experiments were performed on samples of unlabeled Frq1 and Frq1 that contained a ^{13}C-labeled myristoyl group (Figure 7). Because the HSQC experiment selectively probes protons that are covalently attached to ^{13}C, only the methylene and methyl proton resonances of the fatty acyl chain appear in these spectra. Weak extraneous peaks near 0.9, 1.4, and 1.7 ppm (^1H dimension) are due to natural abundance ^{13}C signals from the protein. The spectrum of the N-myristoyl group in Ca^{2+}-free Frq1 (Figure 7, panel B) looks quite similar to the spectrum of free myristic acid in solution (Figure 7, panel A) and the resonance frequencies of corresponding peaks are nearly identical. Assignments of the myristoyl group resonances for Ca^{2+}-free Frq1 (Figure 7, panel B) were therefore derived from assignments of those for free myristic acid, which were determined previously (*22*). The similarity in the spectrum of the N-myristoyl group in Ca^{2+}-free Frq1 to that of free myristic acid in solution indicates that, in Ca^{2+}-free Frq1, the fatty acyl chain is solvent-exposed, in contrast to Ca^{2+}-free recoverin where the myristoyl chain is deeply wedged inside the core of the protein (*19*).

To further test whether the myristoyl group of Frq1 is solvent-exposed, three-dimensional ($^{13}C/F_1$)-edited and ($^{13}C/F_3$)-filtered NOESY experiments *(22)* were performed on unlabeled Frq1 protein containing a ^{13}C-labeled myristate. These spectra selectively probed atoms of residues in the protein that lie within 5 Å of the labeled CH_3 group of the myristoyl chain. NOE dipolar interactions between the myristate methyl group and the protein could not be detected (data not shown). The lack of observable NOEs in this experiment indicates that the methyl group of the fatty acyl chain is more than 5 Å away from atoms in the protein, providing additional support for the conclusion that the N-myristoyl group of Frq1 is solvent-exposed and does not interact intimately with the protein.

The addition of Ca^{2+} to myr-Frq1 caused no discernible change in the NMR spectrum of the myristoyl group (Figure 7, panel C). In addition, NOE interactions between the myristate and the protein could not be detected (data not shown) in three-dimensional ($^{13}C/F_1$)-edited and ($^{13}C/F_3$)-filtered NOESY spectra of Ca^{2+}-bound ^{13}C-myr-Frq1, suggesting that the methyl group of the fatty acyl chain does not interact closely with the Ca^{2+}-bound protein. Hence, the myristoyl group of Ca^{2+}-bound Frq1 appears solvent-exposed and does not undergo a calcium-induced change in environment, in contrast to what has been observed previously in recoverin (*22*).

Subcellular Fractionation of Frq1. To assess the role of Ca^{2+}-induced conformational changes and the N-myristoyl group in the ability of Frq1 to associate with membranes, we examined the distribution of Frq1 (with and without its N-terminal myristoyl modification) in the soluble and particulate fractions of whole-cell extracts (prepared in the presence and absence of Ca^{2+}). For this purpose, either normal myr-Frq1 or a nonmyristoylated mutant, Frq1(G2A), were expressed from plasmids in a yeast cell (*frq1*Δ mutant) lacking the endogenous protein. The resulting extracts were then fractionated by differential centrifugation at successively higher sedimentation rates. In the presence of Ca^{2+}, the

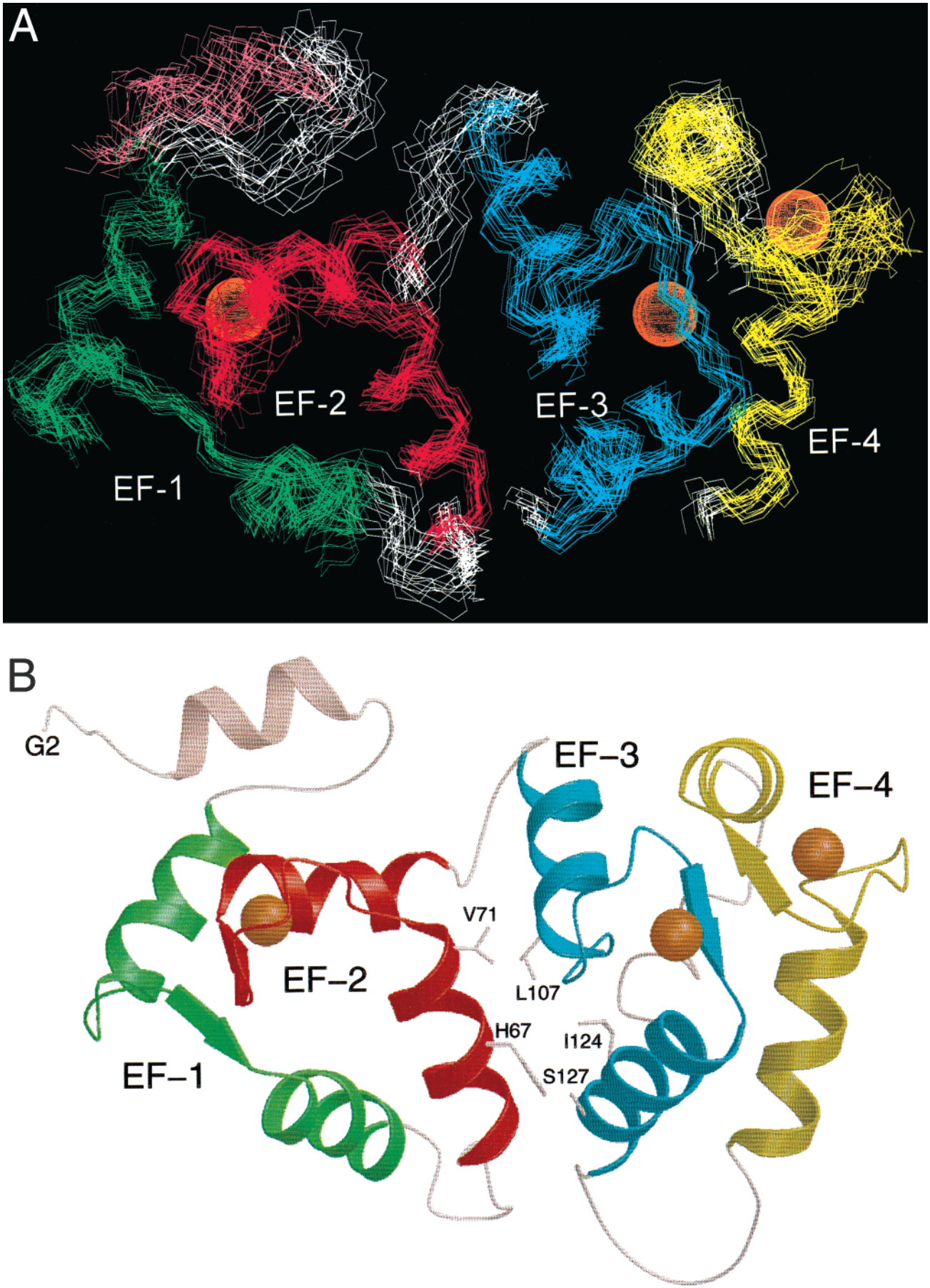

FIGURE 6: Proposed structure of yeast Frq1 based on NMR homology modeling. Superposition of main chain atoms of 20 NMR-derived structures (A) and schematic ribbon diagram of the energy-minimized average structure (B) of unmyristoylated Frq1 with three Ca^{2+} bound. The root-mean-square deviation of the NMR-derived structures relative to the mean structure is 0.9 Å for main chain atoms and 1.5 Å for all non-hydrogen atoms in the regions of regular secondary structure. The coordinates of the structural model of Ca^{2+}-bound Frq1 have been deposited into the Protein Data Bank (1FPW).

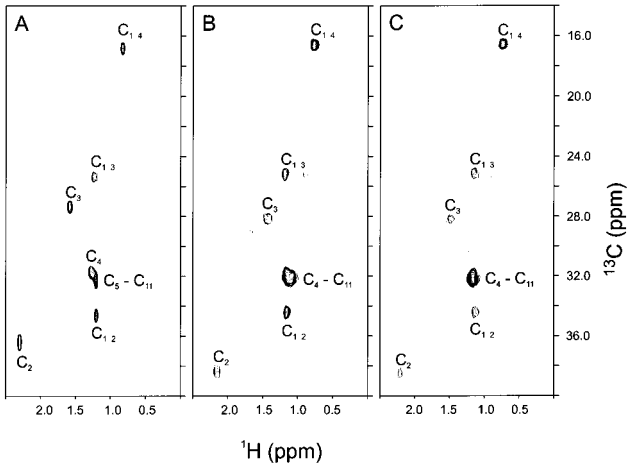

FIGURE 7: The N-myristoyl group of Frq1 appears to be solvent-exposed. Two-dimensional (^{1}H-^{13}C HSQC) NMR spectra of free myristic acid dissolved in chloroform (A) and the myristoyl group of Ca^{2+}-free (B) and Ca^{2+}-bound (C) Frq1. The myristoyl group was labeled with carbon-13, and the protein was unlabeled. The peaks in the spectrum represent protons attached to ^{13}C-labeled fatty acyl chain.

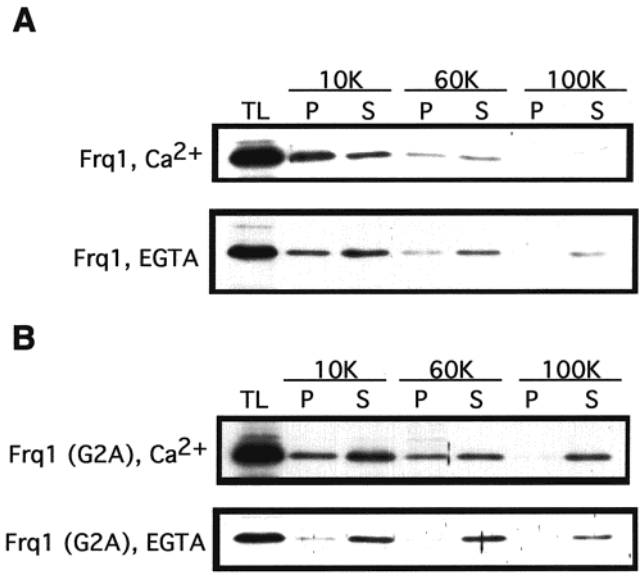

FIGURE 8: Both Ca^{2+}-induced conformational changes and the N-myristoyl group contribute to membrane association of Frq1. Lysates of a *S. cerevisiae frq1*Δ mutant expressing either normal myr-Frq1 (panel A) or a unmyristoylated mutant, Frq1(G2A) (panel B), from the native *FRQ1* promoter on a low copy number (*CEN*) plasmid were prepared, as described in Experimental Procedures, in either the presence of Ca^{2+} or in the presence of excess chelator (EGTA + EDTA), as indicated. After clarification, the resulting extracts (total lysate, TL) were fractionated sequentially by centrifugation at 10000*g*, 60000*g*, and 100000*g*. The resulting pellets (P) and supernatant fractions (S) were resolved by SDS−PAGE, and the presence of Frq1 was detected by immunoblotting with rabbit polyclonal anti-Frq1 antibodies (*10*).

majority of the myr-Frq1 sedimented at 10000*g* (Figure 8, panel A), a particulate fraction known to contain membranes, especially plasma membrane (*46*). After successive sedimentation at 60000*g* and 100000*g*, which removes other cellular membranes and organelles (*47*), just a tiny trace of the Ca^{2+}-bound myr-Frq1 remained in the final 100000*g* supernatant fraction. In contrast, in the absence of Ca^{2+}, much less of the total myr-Frq1 sedimented at 10000*g* and readily detectable amounts of Ca^{2+}-free myr-Frq1 remained in the supernatant fraction of the 100000*g* sedimentation. These same differences were reproducibly observed in three independent trials. Thus, myr-Frq1 partitions much more efficiently with membranes when it is in its Ca^{2+}-bound state than when it is in its Ca^{2+}-free state.

The fractionation behavior of unmyristoylated Frq1(G2A) was markedly different (Figure 8, panel B). Even in the presence of Ca^{2+}, the majority of the protein did not sediment at 10000*g*, and copious amounts remained in the supernatant fraction after the 100000*g* sedimentation. However, in the presence of Ca^{2+}, readily detectable amounts of Frq1(G2A) were still found in the pellet fractions of the 10000*g* and 60000*g* centrifugations. In contrast, in the absence of Ca^{2+}, nearly all of the Frq1(G2A) remained in the supernatant fractions, and only trace amounts were found in the pellets fractions regardless of the sedimentation rate. Again, these patterns were reproducibly observed in three independent trials. Taken together, these findings suggest that the presence of the N-myristoyl group is necessary for high-affinity interaction of Frq1 with biological membranes but that Ca^{2+}-binding induces additional changes that contribute to the ability of Frq1 to associate with membranes in a manner independent of the N-myristoyl moiety.

DISCUSSION

The overall structural similarity between Frq1 and recoverin predicted from the results obtained in our study may not be too surprising given their sequence relatedness. If their structures are so similar, however, how can their nonoverlapping physiological functions be explained? Recoverin is an inhibitor of rhodopsin kinase (*48*, *49*), whereas Frq1 is an activator of phosphatidylinositol 4-kinase (*10*). It has been reported that neuronal calcium sensor-1, the mammalian homologue of vertebrate and invertebrate frequenins and yeast Frq1, can inhibit rhodopsin kinase and some other G-protein-coupled-receptor kinases (or GRKs), at least in vitro (*50*); however, the *S. cerevisiae* genome lacks any clear-cut homologue of the GRK family (*51*). In this regard, it is interesting that residues within the N-terminal region of recoverin (also known as *S*-modulin) have been implicated in the contacts made with rhodopsin kinase (*52*) and that the corresponding residues in Frq1 (Phe22, Glu26, Phe55, and Thr92) are all conserved. Specificity could be provided, of course, by tissue-specific expression of these Ca^{2+}-binding regulatory proteins and/or their target(s). Clearly, however, the structures of both Frq1 and recoverin bound to their docking sites in their respective target proteins will need to be determined to fully understand the selectivity and mechanism of action of these proteins.

One distinct difference between Frq1 and recoverin found in our study is that, at saturation, Frq1 binds three Ca^{2+}, whereas it has been shown previously that recoverin has only two functional Ca^{2+}-binding sites (EF-2 and EF-3). Presumably, the three operational EF-hand motifs in Frq1 (EF-2, EF-3, and EF-4) make its function responsive to changes in Ca^{2+} concentration over a greater dynamic range. Indeed, when EF-4 in recoverin is "repaired" by site-directed mutations that restore its Ca^{2+}-binding ability, the resulting recoverin molecule is reportedly a more effective inhibitor of rhodopsin kinase at lower Ca^{2+} concentrations than normal recoverin (*53*). In this same regard, the temperature-sensitive allele of Frq1, *frq1-1*^{ts}, that was used for many of our physiological studies of Frq1 function in vivo contains four

substitution mutations (F34S, K151E, G162S, and N184Y) and supports cell growth at 26 °C but not at 37 °C (*10*). The first change (F34S) falls in EF-1 and alters a residue that is also conserved in recoverin (Phe35). Two other changes (K151E and G162S) fall in EF-4 of Frq1, but only one of the corresponding residues in recoverin (Lys154 and Asp165) is conserved. The fourth change (N184Y) affects a residue that is similar (Gln187) in recoverin. The four point mutations in the *frq1-1^{ts}* allele were separated using standard methods of molecular biology to determine their contributions to the temperature-sensitive phenotype of the mutant protein (*54*). It was found, first, that the N184Y alteration does not contribute significantly to the instability of the mutant protein because a derivative (*frq1-14*) containing the first three substitutions (F34S, K151E, Gl62S) displayed a temperature-sensitive phenotype equivalent to the original quadruple replacement (*54*). On the basis of our secondary structure analysis (Figure 5) and three-dimensional model (Figure 7), N184 in Frq1 is distal to EF-4 and within a short α-helix at the C-terminus of the protein. Although the triple mutant, F34S K151E G162S (*frq1−14*), was temperature-sensitive, neither F34S alone (*frq1-12*) nor all three C-terminal substitutions alone, K151E G162S N184Y (*frq1-13*), displayed a temperature-sensitive phenotype. Hence, the combination of F34S and either K151E or G162S (or both) are necessary to make the protein nonfunctional at elevated temperature. In our model of Ca^{2+}-bound Frq1, F34 seems to project into a groove that appears to be lined with a cluster of primarily nonpolar residues; hence, the F34S alteration may reduce these hydrophobic interactions and destabilize this region of the protein. Likewise, by analogy to Lys154 in recoverin, which can be seen to form a salt bridge with Asp144 in the high-resolution crystal structure of recoverin (*20*), the equivalent residues in Frq1 (K151 and D141) may interact electrostatically; if so, the K151E alteration would clearly disrupt this interaction and may thus destabilize this region of the protein. Moreover, since K151 is situated within the α-helix that leads into EF-4, it may also alter the Ca^{2+}-binding properties of EF-4. The G162S alteration most likely has an even more pronounced effect on the Ca^{2+} affinity of EF-4 because this substitution changes the conserved central Gly in the Ca^{2+}-binding loop at that site. Hence, G162S may also affect the stability of Frq1, especially in its Ca^{2+}-bound state. In support of this conclusion, it was found that, at a semipermissive temperature (34 °C) where the *frq1-1^{ts}* strain is barely able to survive on medium containing a standard Ca^{2+} concentration (1−2 mM), supplementation of the medium with a high level of exogenous Ca^{2+} (100−200 mM) permitted the mutant cells to grow and to do so at a rate equivalent to wild-type cells (*54*). This rescue was striking because Ca^{2+} at this high level is slightly toxic to the growth of wild-type yeast cells (*55*).

Another apparent difference between Frq1 and recoverin revealed by our study was the finding that the N-myristoyl group is largely solvent-exposed even in Ca^{2+}-free myr-Frq1, whereas it has been shown previously that Ca^{2+}-binding to recoverin is required to induce conformational changes that extrude its N-myristoyl group. Since the NMR spectra shown here were all recorded in the presence of 20 mM octylglucoside (to prevent protein aggregation), it seemed possible that the presence of the detergent was sufficient to "extract" the N-myristoyl group from the body of myr-Frq1, even in the absence of Ca^{2+}. However, NMR spectra of ^{13}C-myristate-labeled myr-Frq1 were recorded in both the absence and the presence of the detergent, and no differences in the spectrum of the fatty acid were observed (J. B. Ames, unpublished results). Hence, the N-myristoyl group of Frq1 appears solvent-exposed even in the absence of detergent, and its disposition is, therefore, not an artifact of the presence of detergent. Conversely, the N-myristoyl group of recoverin remains buried in the interior of the protein, even if detergent is present. The solvent-exposure of the N-myristoyl group of Ca^{2+}-free Frq1 is somewhat unexpected because residues thought to be important for sequestering the N-myristoyl group in Ca^{2+}-free recoverin (W31, I52, and Y53) (*39*) are all conserved in Frq1 (W30, I51, and Y52). Nonetheless, in agreement with the conclusion that the fatty acyl chain is largely exposed in Ca^{2+}-free myr-Frq1, we found that myr-Frq1 was able to associate with membranes even in the absence of Ca^{2+}, although less efficiently than in its Ca^{2+}-bound state. In the present study, we did not find that Ca^{2+}-binding to Frq1 promoted changes that are communicated to the N-myristoyl group; hence, the enhancement of membrane binding observed for Ca^{2+}-bound myr-Frq1 cannot be attributed solely to the N-myristoyl moiety. Indeed, we found that even nonmyristoylated Frq1 was able to associate with membranes to some degree, as long as Ca^{2+} was present. Only nonmyristoylated Frq1 in the absence of Ca^{2+} failed to show significant membrane-binding ability. These findings suggest that the Ca^{2+}-induced conformational changes in Frq1 that we have demonstrated in this study increase its propensity to interact with a hydrophobic surface by means independent of the N-myristoyl group. One plausible mechanism for the Ca^{2+}-induced enhancement of membrane-binding ability even in the absence of the fatty acyl chain would be via conformational changes that expose nonpolar side chains that are buried in the Ca^{2+}-free form of Frq1. In recoverin, it has been shown that Ca^{2+}-binding not only causes conformational changes that extrude the N-myristoyl group but that also expose a number of formerly buried hydrophobic side chains (*19*, *52*). Indeed, in our structural model of Ca^{2+}-bound Frq1 (Figure 6), a number of conserved hydrophobic side chains cluster to form a solvent-exposed patch (F22, W30, Y52, F55, F56, F85, and L89).

Of course, it is possible that Frq1 contains some additional lipophilic substituent in addition to its N-myristoyl group. A 24-kDa Ca^{2+}-binding protein associated with the flagellum in the protozoan, *Trypanosoma cruzi*, is both N-myrisytoylated and *S*-palmitoylated near its N-terminus, and elimination of both modifications is required to prevent membrane association of the protein (*56*). Frq1 has only two cysteine residues; one (Cys38) is situated within the loop of EF-1, but the other (Cys15) lies quite near the N-terminus of Frq1. Of course, the myr-Frq1 used in our NMR studies was prepared in *E. coli* coexpressing an N-myristoyltransferase and did not contain any other modification, as judged by electrospray ionization mass spectrometry of the purified protein (D. S. King, B. Q. Wang, and J. Thorner, unpublished results). However, the cell fractionation experiments were performed with extracts of yeast cells. We have already demonstrated that the nonmyristoylated Frq1(G2A) mutant is capable of restoring viability to a *frq1*Δ cell (*10*), in agreement with our observation that, in the presence of Ca^{2+}, even unmyristoylated Frq1 shows residual ability to associate

with membranes (Figure 8). To address the issue of the potential role of Cys15 modification, we generated a Frq1-(G2A C15A) double mutant and found that it is able to support growth of *frq1-1^{ts}* cells at an otherwise nonpermissive temperature, suggesting that neither Cys15 nor its S-palmitoylated are required (even in the absence of the N-myristoyl group) for the in vivo physiological function of Frq1 (I. G. Huttner and J. Thorner, unpublished results).

Finally, there is evidence that, in addition to the N-myristoyl group, basic residues in the C-terminal "tail" of recoverin (eight positively charged side chains in the last 23 residues distal to EF-4) are important for the high-affinity binding of recoverin to membranes (*57*). Such a mechanism cannot be involved in the targeting of Frq1 to membranes because the C-terminus of Frq1 beyond EF-4 is totally devoid of basic residues.

ACKNOWLEDGMENT

We thank Dr. Bo Qing Wang for advice and contribution of materials and Frank Delaglio and Dan Garrett for writing computer software for NMR data processing and analysis.

REFERENCES

1. Davis, T. N. (1995) *Adv. Second Messenger Phosphoprotein Res. 30*, 339−358.
2. Berridge, M. J. (1997) *J. Physiol. 499*, 291−306.
3. Fischer, M., Schnell, N., Chattaway, J., Davies, P., Dixon, G., and Sanders, D. (1997) *FEBS Lett. 419*, 259−262.
4. Catty, P., and Goffeau, A. (1996) *Biosci. Rep. 16*, 75−85.
5. Ikura, M. (1996) *Trends Biochem. Sci. 21*, 14−17.
6. Davis, T. N., Urdea, M. S., Masiarz, F. R., and Thorner, J. (1986) *Cell 47*, 423−431.
7. Baum, P., Furlong, C., and Byers, B. (1986) *Proc. Natl. Acad. Sci. U.S.A. 83*, 5512−5516.
8. Cyert, M. S., and Thorner, J. (1992) *Mol. Cell. Biol. 12*, 3460−3469.
9. Stevens, R. C., and Davis, T. N. (1998) *J. Cell Biol. 142*, 711−722.
10. Hendricks, K. B., Wang, B. Q., Schnieders, E. A., and Thorner, J. (1999) *Nat. Cell Biol. 1*, 234−241.
11. Braunewell, K. H., and Gundelfinger, E. D. (1999) *Cell Tissue Res. 295*, 1−12.
12. Palczewski, K., Polans, A. S., Baehr, W., and Ames, J. B. (2000) *BioEssays 22*, 337−350.
13. Hama, H., Schnieders, E. A., Thorner, J., Takemoto, J. Y., and DeWald, D. B. (1999) *J. Biol. Chem. 274*, 34294−34300.
14. Walch-Solimena, C., and Novick, P. (1999) *Nat. Cell Biol. 1*, 523−525.
15. McFerran, B. W., Graham, M. E., and Burgoyne, R. D. (1998) *J. Biol. Chem. 273*, 22768−22772.
16. Jeromin, A., Shayan, A. J., Msghina, M., Roder, J., and Atwood, H. L. (1999) *J. Neurobiol. 41*, 165−175.
17. Kawasaki, H., Nakayama, S., and Kretsinger, R. H. (1998) *Biometals 11*, 277−295.
18. Yap, K. L., Ames, J. B., Swindells, M. B., and Ikura, M. (1999) *Proteins 37*, 499−507.
19. Ames, J. B., Ishima, R., Tanaka, T., Gordon, J. I., Stryer, L., and Ikura, M. (1997) *Nature 389*, 198−202.
20. Hughes, R. E., Brzovic, P. S., Klevit, R. E., and Hurley, J. B. (1995) *Biochemistry 34*, 11410−11416.
21. Tanaka, T., Ames, J. B., Harvey, T. S., Stryer, L., and Ikura, M. (1995) *Nature 376*, 444−447.
22. Ames, J. B., Tanaka, T., Ikura, M., and Stryer, L. (1995) *J. Biol. Chem. 270*, 30909−30913.
23. Ames, J. B., Tanaka, T., Stryer, L., and Ikura, M. (1996) *Curr. Opin. Struct. Biol. 6*, 432−438.
24. Sanada, K., Shimizu, F., Kameyama, K., Haga, K., Haga, T., and Fukada, Y. (1996) *FEBS Lett. 384*, 227−230.
25. Lange, C., and Koch, K. W. (1997) *Biochemistry 36*, 12019−12026.
26. Duronio, R. J., Rudnick, D. A., Johnson, R. L., Linder, M. E., and Gordon, J. I. (1990) *Methods 1*, 253−263.
27. Muchmore, D. C., McIntosh, L. P., Russell, C. B., Anderson, D. E., and Dahlquist, F. W. (1989) *Methods Enzymol. 177*, 44−86.
28. McIntosh, L. P., and Dahlquist, F. W. (1990) *Q. Rev. Biophys. 23*, 1−38.
29. Ames, J. B., Tanaka, T., Stryer, L., and Ikura, M. (1994) *Biochemistry 33*, 10743−10753.
30. Tanaka, T., Ames, J. B., Kainosho, M., Stryer, L., and Ikura, M. (1998) *J. Biomolec. NMR 11*, 135−152.
31. Brünger, A. T. (1992) *X-PLOR, Version 3.1: A System for X-ray Crystallography and NMR*, Yale University Press, New Haven, CT.
32. Badger, J., Kumar, R. A., Yip, P., and Szalma, S. (1999) *Proteins 35*, 25−33.
33. Bagby, S., Harvey, T. S., Eagle, S. G., Inouye, S., and Ikura, M. (1994) *Structure 2*, 107−122.
34. Brooks, S. P., and Storey, K. B. (1992) *Anal. Biochem. 201*, 119−126.
35. Ladant, D. (1995) *J. Biol. Chem. 270*, 3179−3185.
36. Paulus, H. (1969) *Anal. Biochem. 32*, 91−100.
37. Vijay-Kumar, S., and Kumar, V. D. (1999) *Nat. Struct. Biol. 6*, 80−88.
38. Ames, J. B., Ikura, M., and Stryer, L. (2000) *Methods Enzymol. 316*, 121−132.
39. Baldwin, A. N., and Ames, J. B. (1998) *Biochemistry 37*, 17408−17419.
40. Ames, J. B., Porumb, T., Tanaka, T., Ikura, M., and Stryer, L. (1995) *J. Biol. Chem. 270*, 4526−4533.
41. Freifelder, D. (1982) in *Physical Biochemistry: Applications to Biochemistry and Molecular Biology*, pp 537−572, W. H. Freeman and Company, San Francisco, CA.
42. Wishart, D. S., Sykes, B. D., and Richards, F. M. (1992) *Biochemistry 31*, 1647−1651.
43. Ames, J. B., Dizhoor, A. M., Ikura, M., Palczewski, K., and Stryer, L. (1999) *J. Biol. Chem. 274*, 19329−19337.
44. Babu, Y. S., Bugg, C. E., and Cook, W. J. (1988) *J. Mol. Biol. 204*, 191−204.
45. Herzberg, O., and James, M. N. (1988) *J. Mol. Biol. 203*, 761−779.
46. Panaretou, B., and Piper, P. (1996) *Methods Mol. Biol. 53*, 117−121.
47. Lupashin, V. V., Hamamoto, S., and Schekman, R. W. (1996) *J. Cell Biol. 132*, 277−289.
48. Klenchin, V. A., Calvert, P. D., and Bownds, M. D. (1995) *J. Biol. Chem. 270*, 16147−16152.
49. Chen, C. K., Inglese, J., Lefkowitz, R. J., and Hurley, J. B. (1995) *J. Biol. Chem. 270*, 18060−18066.
50. Iacovelli, L., Sallese, M., Mariggio, S., and de Blasi, A. (1999) *FASEB J. 13*, 1−8.
51. Hunter, T., and Plowman, G. D. (1997) *Trends Biochem. Sci. 22*, 18−22.
52. Tachibanaki, S., Nanda, K., Sasaki, K., Ozaki, K., and Kawamura, S. (2000) *J. Biol. Chem. 275*, 3313−3319.
53. Alekseev, A. M., Shulga-Morskoy, S. V., Zinchenko, D. V., Shulga-Morskaya, S. A., Suchkov, D. V., Vaganova, S. A., Senin, I. I., Zargarov, A. A., Lipkin, V. M., Akhtar, M., and al., e. (1998) *FEBS Lett. 440*, 116−118.
54. Hendricks, K. B. (1999) Ph.D. Thesis, University of California, Berkeley.
55. Tanida, I., Hasegawa, A., Iida, H., Ohya, Y., and Anraku, Y. (1995) *J. Biol. Chem. 270*, 10113−10119.
56. Godsel, L. M., and Engman, D. M. (1999) *EMBO J. 18*, 2057−2065.
57. Matsuda, S., Hisatomi, O., and Tokunaga, F. (1999) *Biochemistry 38*, 1310−1315.

BI0012890